Progress In Electromagnetics Research Letters, Vol. 82, 41–49, 2019

Higher-Order Moving Target Detection for Rotating Scanning Synthetic Aperture Interferometric Radiometer

Jianfei Chen[1, 2, *], Sheng Zhang[1], and Xiaowei Zhu[2]

Abstract—Since passive millimeter wave synthetic aperture interferometric radiometer (SAIR) has the advantages of high spatial-resolution and large field of view, it is an attractive tool for wide area surveillance. Among the SAIRs, the Rotating Scanning SAIR (RS-SAIR) with linear sparse array is a popular system with low redundancy and high reliability. According to the detection mechanism of RS-SAIR, we extend RS-SAIR to deal with higher-order moving target detection (HMTD) for the first time in this paper. In the proposed HMTD method, the 2D time-projection image is constituted by the 1D projection images measured by RS-SAIR firstly. Then, the projection trajectory of moving target can be extracted from the time-projection image. Finally, the positions and motion parameters are estimated by fitting the moving target's trajectory. Simulation results indicate that the position and motion parameters of higher-order moving target can be well estimated with high real time and accuracy by the proposed HMTD method.

1. INTRODUCTION

Moving target detection is very important for many applications such as target tracking or classification, vehicle trajectory determination, and others [1–4]. The traditional moving target detecting methods can be generally divided into two categories: image sequences based methods and echo signals based methods. The image sequences based methods detect the moving target by analyzing the target positions extracted from images [3–5]. Obviously, image sequences of whole target scene required to be primarily measured during the target motion, the information and algorithm complexity of these methods are usually large, and its real-time performance is poor. Echo signals based methods detect the moving target by analyzing the detector echo signals, which contains the position and motion information of moving target. This is the main method for moving target detection, which is widely used in airborne or satellite-borne radar (such as Doppler radar and SAR) [6–10]. Using the echo signals based methods with small information and algorithm complexity, the high real-time detection of moving target can be easily achieved. However, traditional echo signals based methods mainly deal with simple moving targets with steady velocity and are unsuitable for detecting the higher-order moving target with accelerated velocity and veer. In addition, echo signals based methods require the detection system to emit signals actively. As a result, the stealth performance of detection system is poor, and the stealth target covered with absorption material cannot be detected effectively.

Millimeter wave synthetic aperture interferometric radiometer (SAIR) is a powerful passive detection system for high-resolution surveillance and has been used in various applications [11–14]. Since the SAIR passively receives the target natural radiation, it can effectively overcome the influence of absorbing material, achieving stealth target detection. Among the SAIRs, the Rotating Scanning SAIR

Received 28 November 2018, Accepted 3 January 2019, Scheduled 6 March 2019

* Corresponding author: Jianfei Chen (chenjf@njupt.edu.cn).

[1] Optical Engineering, Nanjing University of Posts and Telecommunications, Nanjing 210003, China. [2] School of Information Science and Engineering, Southeast University, Nanjing 210096, China.

(RS-SAIR) with linear sparse array is a popular system with low redundancy and high reliability [14–19]. By rotating the linear sparse array, RS-SAIR uses fewer antennas to achieve the high-resolution and large field of view (FOV) imaging observation. However, limited by the scanning imaging system, its 2D imaging time is long. Moreover, the sampling points of RS-SAIR is subjected to circularly distribution, which is unsuitable for the traditional FFT model based imaging methods. To deal with these irregular samples, some irregular imaging methods (such as Gridding and NUFFT) were proposed for RS-SAIR [20–23]. But the imaging accuracy of these methods is low, and the unnecessary error is introduced when resampling and interpolating the visibility function. Some researches [24, 25] show that the key to achieve high-precision imaging is to find the appropriate inverse method to reconstruct the target images from the visibility function directly.

Although 2D imaging performance of RS-SAIR is poor, it can measure the 1D projection image which contains moving target information in real time. This indicates that RS-SAIR has the potential to be used for moving target detection. In RS-SAIR, with the rotation of antenna array, the radial visibility function is measured by linear sparse array in real time. The measured visibility function is equispaced in radial direction and suitable for applying FFT, and the 1D projection images can be reconstructed by FFT-methods from the radial visibility function directly. More importantly, the projection information of moving target in the 1D projection images changes regularly when performing the array rotation. Based on this fact, the position and motion parameters of moving target may be detected by analyzing the 1D projection images of RS-SAIR. According to the detection mechanism of RS-SAIR, we extend RS-SAIR to handle higher-order moving target detection (HMTD) for the first time in this paper. In the proposed HMTD method, 1D projection images are firstly reconstructed to form a 2D time-projection image. Then, the projection trajectory of moving target can be extracted from the time-projection image. Finally, the position and motion parameters will be estimated by fitting the moving target's trajectory. Different from 2D imaging of RS-SAIR, the detection of moving target is realized by analyzing the 1D projection images in HMTD method, which can effectively overcome the RS-SAIR's disadvantages (long imaging time) and maintain its advantages (large FOV and high resolution). The simulation results indicate that HMTD method can estimate motion parameters of higher-order moving target accurately and achieve real-time target tracking for RS-SAIR.

2. THE BASIC SYNTHESIS APERTURE IMAGING THEORY

Before the description of HMTD method for RS-SAIR, the basic synthesis aperture imaging theory is demonstrated here. As shown in Fig. 1, the antennas are located on OXY, and the extend radiation source S is located on oxy, whose brightness temperature image is $T(x, y)$. The radiation source S is dispersed into N small parts. The distances between the i-th radiation source S_i and antennas c and l are R_i^c and R_i^l, respectively.

The correlation between the received signals E_c and E_l of pairwise antennas (c, l) is a sample of the so called visibility function. According to [26], the visibility samples measured by pairwise antennas

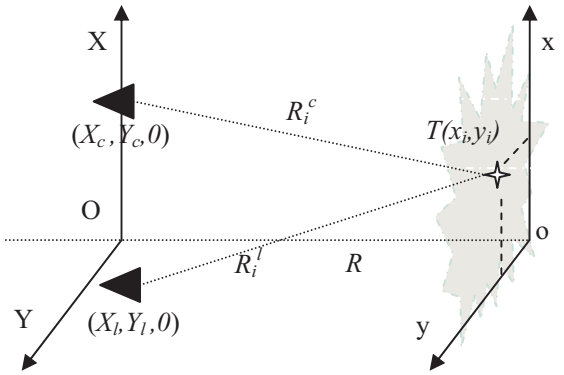

Figure 1. Geometry diagram of 2D synthetic aperture imaging.

(c,l) can be expressed as

$$V_{c,l} = \left\langle E_c\left(R_i^c,t\right)\cdot E_l^*\left(R_i^l,t\right)\right\rangle = \sum_{i=1}^{N} T(x_i,y_i)F_c(x_i,y_i)F_l^*(x_i,y_i)r_{c,l}e^{-jk\left(R_i^c-R_i^l\right)} \tag{1}$$

where $\langle\cdot\rangle$ denotes time integration operation, (x_i,y_i) the coordinate of the point target S_i, T the normalized brightness temperature, $F(\cdot)$ the normalized antenna pattern, $k=2\pi/\lambda$ the circular wave number, and $r_{c,l}$ the so called fringe-wash function [27]. $\exp[-jk(R_i^c-R_i^l)]$ denotes the phase difference of two antennas, which is the key factor for the synthetic aperture imaging. According to Fig. 1, distances R_i^c and R_i^l through Taylor expansion can be expressed as

$$R_i^c = \sqrt{(x_i-X_c)^2+(y_i-Y_c)^2+R^2} \approx R+\left[(x_i-X_c)^2+(y_i-Y_c)^2\right]/2R \tag{2}$$

$$R_i^l \approx R+\left[(x_i-X_l)^2+(y_i-Y_l)^2\right]/2R \tag{3}$$

Substitute Equations (2) and (3) into Equation (1), and define the spatial coordinates $u=k(X_l-X_c)/R$, $v=k(Y_l-Y_c)/R$. We can get the relation between visibility function, and the brightness temperature image is as follows.

$$V(u,v) = e^{-j\varphi(u,v)}\iint T(x,y)F_cF_l^*r_{c,l}e^{-j(xu+yv)}dxdy \tag{4}$$

where $\varphi(u,v)=k(X_c^2+Y_c^2-X_l^2-Y_l^2)/2R$ is the phase-modified item, which can improve the imaging accuracy for the near-field SAIR effectively. For the ideal SAIR with identical receivers and antennas, the decorrelation effects $r_{c,l}\approx 1$ and antenna pattern $F(\cdot)$ can be ignored simply. Then Equation (4) can be further simplified as follows

$$V(u,v) = e^{-j\varphi(u,v)}\iint T^O(x,y)e^{-j(xu+yv)}dxdy \tag{5}$$

$$T^O(x,y) = \iint\left[V(u,v)e^{j\varphi(u,v)}\right]e^{j(xu+yv)}dudv \tag{6}$$

where $T^O(x,y)$ is the approximate brightness temperature image. For a complete visibility function $V(u,v)$ with standard rectangular distribution, the brightness temperature image $T^O(x,y)$ can be reconstructed by the FFT-based methods as an approximate solution of $T(x,y)$. For the Modified-FFT (MFFT) imaging method, the brightness temperature images are reconstructed by Fourier transform from the visibility function with phase-modified item directly [28].

$$T = FT_2\left[V(u,v)e^{j\varphi(u,v)}\right] \tag{7}$$

3. DESCRIPTION OF HMTD METHOD FOR RS-SAIR

RS-SAIR uses a linear array that consists of a few antennas to realize high-resolution 2D imaging surveillance. The signal processing and imaging process of RS-SAIR are different from traditional SAIRs. In this section, the proposed HMTD method will be analyzed by combining the imaging mechanism of RS-SAIR. The geometry diagram of RS-SAIR with linear array is shown in Fig. 2. The sparse array is placed in XOY plane and rotated around point O. θ_a is the array rotation angle. The moving target (MT) is placed in xoy plane, and its coordinate is (x_{MT}, y_{MT}).

For the sparse array with given θ_a, set the array direction as X_p-axis, constructing a projection coordinate system (X_pOY_p), which moves with the rotation of array angle θ_a. Under the coordinate X_pOY_p, the spatial coordinates of antennas are $u=k(X_l-X_c)/R$, $v=k(Y_l-Y_c)/R=0$, and the coordinates of targets should be transformed to (x_p,y_p). Then the visibility function $V_{\theta a}(u,v)$ measured by the sparse array at given θ_a can be rewritten as

$$\begin{aligned} V_{\theta a}(u,0) &= e^{-j\varphi(u,0)}\iint T(x_p,y_p)e^{j(x_pu+y_p0)}dx_pdy_p \\ V_{\theta a}(u)e^{j\varphi(u)} &= \int\left[\int T(x_p,y_p)dy_p\right]e^{-j(x_pu)}dx_p = \int T_{\theta a}^P(x_p)e^{-j(x_pu)}dx_p \end{aligned} \tag{8}$$

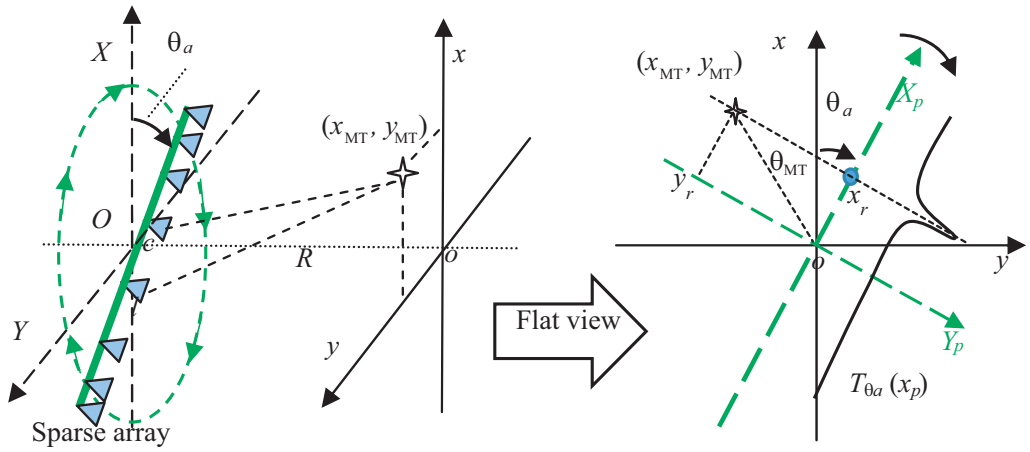

Figure 2. Geometry diagram of rotating scanning synthetic aperture imaging.

where x_p is the projection coordinate on the X_p-axis (paralleling to the sparse array at angle θ_a), and y_p is the projection coordinate on the Y_p-axis. $T_{\theta a}^P(x_p) = \int T(x_p, y_p)dy_p$ is the 1D projection image, which can be reconstructed by the 1D MFFT method as in the following formula.

$$T_{\theta a}^P(x_p) = FT_1\left[V_{\theta a}(u)e^{j\varphi(u)}\right] \tag{9}$$

Generally, the 1D projection images with different θ_a can be used to reconstruct the brightness temperature image T. However, this paper is dedicated to detecting the moving targets, and the 1D projection images are directly used to detect the moving target's position. For a given target MT, when the array rotates with a constant angle velocity ω, its projection coordinates $x_{p\text{-MT}}$ in 1D projection image can be expressed as

$$x_{p\text{-MT}}(t) = R_{\text{MT}}(t)\cos(\omega t + \theta_{a0} + \theta_{\text{MT}}(t)) \tag{10}$$

$$\begin{aligned} R_{\text{MT}}(t) &= \sqrt{x_{\text{MT}}^2(t) + y_{\text{MT}}^2(t)} \\ \theta_{\text{MT}}(t) &= \arctan\left[x_{\text{MT}}(t)/y_{\text{MT}}(t)\right] \end{aligned} \tag{11}$$

where θ_{a0} is the initial angle of array, and $(x_{\text{MT}}(t), y_{\text{MT}}(t))$ is the coordinate of MT in xoy coordinates at different times. For simplicity, we mainly analyze the moving target with the following motion model in this paper. It can be easily extended to the n-order motion model.

$$\begin{aligned} x_{\text{MT}}(t) &= a_x t^2 + v_x t + x_0 \\ y_{\text{MT}}(t) &= a_y t^2 + v_y t + y_0 \end{aligned} \tag{12}$$

where $[a_x, v_x, x_0, a_y, v_y, y_0]$ are the motion parameters that need to be estimated. It is worth noting that the trajectory $x_{p\text{-MT}}(t)$ of any MT is a continuous function, which can be represented by a polynomial function. Thus, it is reasonable that the higher-order moving targets with n-order motion model can also be estimated by HMTD method accurately.

According to Equations (10), the projection coordinate $x_{p\text{-MT}}(t)$ of MT will be changed with array rotating as $\theta_a = \omega t + \theta_{a0}$, and its trajectory meets the cosine distribution which is modulated by MT's motion parameters. Based on this fact, we can arrange the 1D projection images (with different θ_a) to constitute the time-projection image T_{t-p}. Then, the motion parameters of MT will be extracted by the proposed HMTD method. Its detailed process are as follows:

1) Reconstruct the 1D projection images $T_{\theta a}$ with array rotating, then arrange them to form the time-projection image T_{t-p} according to their measurement time or angle θ_a.
2) Extract the projection coordinates $x_{p\text{-MT}}$ from the image T_{t-p} after subtracting the ground noise.
3) Construct the MT's trajectory equation $x_{p\text{-MT}}(t)$ according to Equations (10)–(12).

4) Fit the extracted projection coordinates $x_{p\text{-MT}}$ to MT's trajectory equation $x_{p\text{-MT}}(t)$ for obtaining the motion parameters of MT.

In the above analysis, we assume that MT's background is a clean background. However, for the real scene, there is some interference in the background, which reduces the extraction accuracy of MT's trajectory. According to the imaging characteristics of RS-SAIR, image T_{t-p} of stationary background is a periodic image with array rotating. Thus, we can subtract the projection image of background from image T_{t-p} before extracting the projection coordinates in step 2 for the complex real scenes. In addition, 1D projection images $T_{\theta a}$ are reconstructed by MFFT method which includes a phase-modified item. Thus, the proposed HMTD method can be applied not only to the far field, but also to the near field target tracking.

4. THE EXPERIMENTS AND RESULTS

To evaluate the performance of proposed HMTD method, two simulation experiments are performed in this section. The main simulation parameters are listed in Table 1.

Table 1. Simulation parameters of RS-SAIR with sparse array.

Parameters	Value	Parameters	Value
Antenna number	16	Wavelength λ	3 mm
Baseline spacing Δu	1.1 cm	Detection distance R	5000 m
Synthetic aperture D_{SA}	1 m	Angle velocity ω	1 rad/s

As shown in Table 1, the RS-SAIR only needs 16 antennas to constitute the sparse linear array. The antennas' locations are set based on references [29], and its position arrangement is shown in Fig. 3. The minimum baseline spacing Δu is 1.1 cm, and the synthesis aperture is about $D_{SA} = 90\Delta u = 1$ m. In this case, the spatial resolution and aliasing free FOV of RS-SAIR are about:

$$\rho = R\lambda/D_{SA} = 15\,\text{m} \tag{13}$$

$$\text{FOV} = R\lambda/\Delta u = 1364\,\text{m} \tag{14}$$

In our simulation, the polarization direction of antennas is assumed to be fixed during the array rotation, which can be achieved by the rotation of antennas regularly with the array rotation. The initial angle θ_{a0} is set as 0. For simulating RS-SAIR's imaging process accurately, the received signals of antennas are obtained by integral operation of the radiation waves generated by all radiation sources. Then, the visibility samples are calculated by cross-correlated calculation between antennas. The 1D projection images $T_{\theta a}$ are reconstructed by FFT method according to Equation (9). As shown in Figs. 4–5, two simulation experiments with aerial target (airplane) and ground target (car) are carried out respectively. The motion parameters of MT are set as [40 m/s^2, -60 m/s, 60 m; 20 m/s^2, 40 m/s, 30 m].

It can be seen from the simulation results that the MT's projection trajectory of airplane is very clear and satisfies cosine distribution in image T_{t-p} (Fig. 4(b)). Although the background of car scene

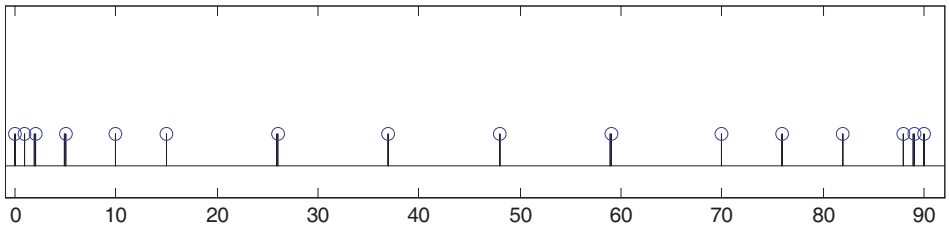

Figure 3. The arrangement of linear sparse array (abscissa unit is Δu).

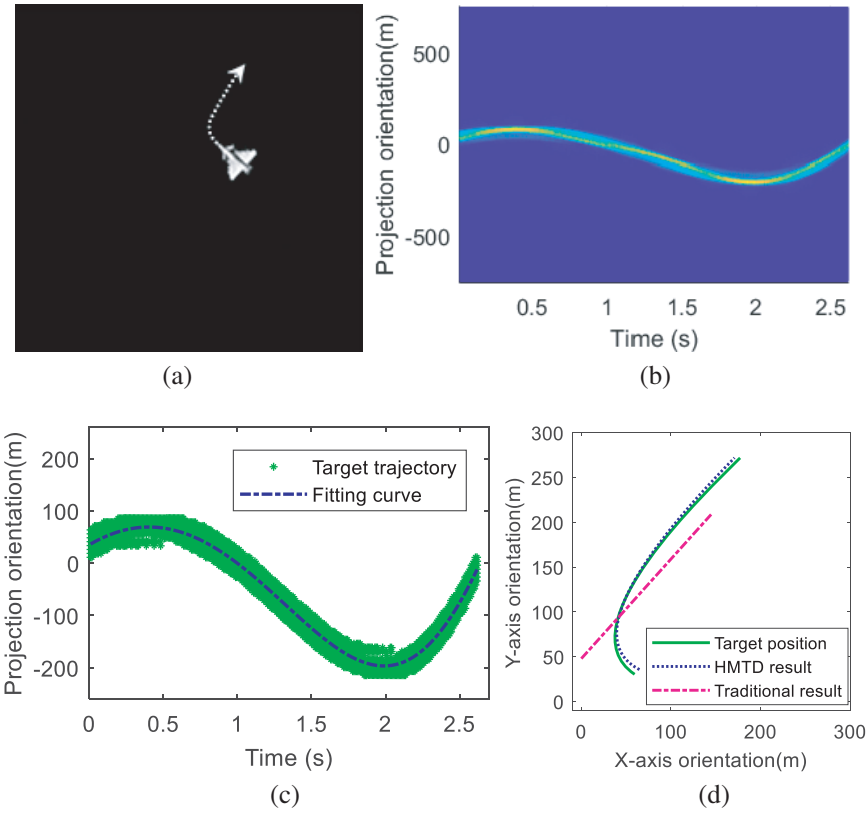

Figure 4. The simulation results of aerial target (airplane). (a) Airplane scene. (b) Time-projection image T_{t-p}. (c) Fitting result of $x_{p\text{-MT}}(t)$. (d) Estimation result.

is complex, its projection trajectory is still clear after the background subtraction as shown in Fig. 5(b). According to these projection coordinates, MT's trajectory equation $x_{r\text{-MT}}(t)$ with motion parameters can be well fitted out by HMTD method as shown in Figs. 4–5(c). The estimated parameters are [39.0, −61.2, 63.9; 21.7, 33.5, 35.4] and [38.5, −60.3, 65.3; 20.7, 34.6, 38.3] for airplane and car scene, respectively. For comparison, traditional detection method with first order motion model is also utilized, and the estimated parameters are [55.5, −0.5; 61.6 47.3] and [56.7, −0.5; 62.1, 49.3], respectively. Obviously, the estimated parameters of HMTD are very close to the real motion parameters of MT, and the estimation error of traditional method is very large. Finally, the MT's trajectory can be drawn according to the estimated parameters and its motion model. As shown in Figs. 4–5(d), the MT's trajectory is able to obtain a more accurate reconstruction by HMTD method. However, because the motion model of traditional method is too simple, its reconstruction error is very large for the higher-order moving target with accelerated velocity.

For an objective comparison, the RMSE of MT's position (as shown in Figs. 4–5(d)) is calculated as

$$\text{RMSE}\left((x,y)^E,(x,y)^T\right)=\int_\tau \frac{\sqrt{[x^E(t)-x^T(t)]^2+[y^E(t)-y^T(t)]^2}}{\sqrt{x^T(t)^2+y^T(t)^2}}dt \tag{15}$$

where $(x,y)^E$ is the estimated position, and $(x,y)^T$ is the real position of MT.

As shown in Table 2, the position error (RMSE) of the traditional method is very large, but the RMSE of HMTD method is very small both for airplane and car scene. This indicates that the proposed HMTD method can track higher-order moving target effectively. In addition, for verifying the real-time performance of proposed HMTD method, the execution time is evaluated on a PC with i7-6700 processor. After data collection, the execution times of HMTD method is 71 ms and 79 ms for airplane and car scene, respectively. This shows that the proposed HMTD method can meet the real-time requirements of moving target tracking.

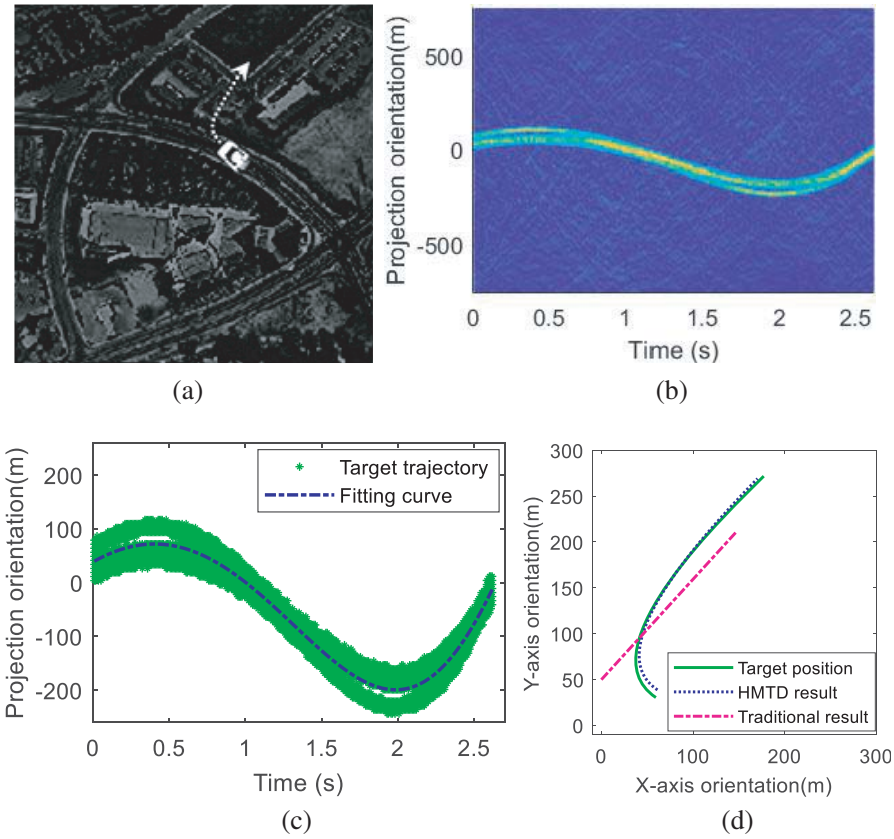

Figure 5. The simulation results of aerial target (car). (a) Car scene. (b) Time-projection image T_{t-p}. (c) Fitting result of $x_{p\text{-MT}}(t)$. (d) Estimation result.

Table 2. Simulation parameters of RS-SAIR with sparse array.

Target scene	RMSE of traditional method	RMSE of HMTD method
Airplane	3.97%	0.05%
Car	3.99%	0.10%

5. CONCLUSION

RS-SAIR with linear sparse array is a popular system with low redundancy and high reliability. According to the detection mechanism of RS-SAIR, we show a novel HMTD method for RS-SAIR to track moving target in real time. In HMTD method, 1D projection images are reconstructed by the MFFT method with array rotating firstly. Then, the 1D projection images are arranged to constitute a 2D time-projection image T_{t-p}. Finally, the positions and motion parameters of moving target are extracted by fitting the moving target's trajectory in image T_{t-p}. Simulation results indicate that HMTD method can track higher-order moving target very well. Furthermore, HMTD method can also be implemented to track the target with time-varying motion parameters, as long as selecting the nearest time images $T_{\theta a}$ to compose image T_{t-p} and then fit the moving target's trajectory in image T_{t-p}.

ACKNOWLEDGMENT

The authors would like to thank the anonymous reviewer and editors for their helpful comments and suggestions. This work was supported by the National Natural Science Foundation of China (61601237, 61671149), Natural Science Foundation of Jiangsu Province (BK20160901), Natural Science Research of Jiangsu Higher Education Institutions (16KJB420001) and NUPTSF (NY215042).

REFERENCES

1. Yamaguchi, R., S. Kidera, and T. Kirimoto, "Accurate imaging method for moving target with arbitrary shape for multi-static UWB radar," *IEICE Transactions on Communications*, Vol. E96b, 2014–2023, Jul. 2013.
2. Wang, L. B., D. W. Wang, J. J. Li, J. Xu, C. Xie, and L. Wang, "Ground moving target detection and imaging using a virtual multichannel scheme in HRWS mode," *IEEE Transactions on Geoscience and Remote Sensing*, Vol. 54, 5028–5043, Sep. 2016.
3. Deng, L. Z. and H. Zhu, "Moving point target detection based on clutter suppression using spatiotemporal local increment coding," *Electronics Letters*, Vol. 51, 626–627, Apr. 16, 2015.
4. Minaeian, S., J. Liu, and Y. J. Son, "Effective and efficient detection of moving targets from a UAV's camera," *IEEE Transactions on Intelligent Transportation Systems*, Vol. 19, No. 2, 497–506, 2018.
5. Wan, M. J., G. H. Gu, W. X. Qian, K. Ren, Q. Chen, H. Zhang, et al., "Total variation regularization term-based low-rank and sparse matrix representation model for infrared moving target tracking," *Remote Sensing*, Vol. 10, No. 4, 510, Apr. 2018.
6. Nanzer, J. A., "Millimeter-wave interferometric angular velocity detection," *IEEE Transactions on Microwave Theory and Techniques*, Vol. 58, 4128–4136, Dec. 2010.
7. Xia, B., J. Xu, Y. N. Peng, and X. G. Xia, "Doppler ambiguity resolving for SAR moving targets via linear migration correction," *Electronics Letters*, Vol. 47, 464–465, 2011.
8. Waqas, M., S. Kidera, and T. Kirimoto, "PCA-based detection algorithm of moving target buried in clutter in doppler frequency domain," *IEICE Transactions on Communications*, Vol. E94b, 3190–3194, Nov. 2011.
9. Yang, J., C. Liu, and Y. F. Wang, "Detection and imaging of ground moving targets with real SAR data," *Ieee Transactions on Geoscience and Remote Sensing*, Vol. 53, 920–932, Feb. 2015.
10. Li, J., Y. Huang, G. S. Liao, and J. W. Xu, "Moving target detection via efficient ATI-GoDec approach for multichannel SAR system," *IEEE Geoscience and Remote Sensing Letters*, Vol. 13, 1320–1324, Sep. 2016.
11. Zhang, Y. L., W. Miao, Z. H. Lin, H. Gao, and S. C. Shi, "Millimeter-wave InSAR image reconstruction approach by total variation regularized matrix completion," *Remote Sensing*, Vol. 10, No. 7, 1053, Jul. 2018.
12. Demirci, S., H. Cetinkaya, E. Yigit, C. Ozdemir, and A. A. Vertiy, "A study on millimeter-wave imaging of concealed objects: Application using back-projection algorithm," *Progress In Electromagnetics Research*, Vol. 128, 457–477, 2012.
13. Appleby, R. and R. N. Anderton, "Millimeter-wave and submillimeter-wave imaging for security and surveillance," *Proceedings of the IEEE*, Vol. 95, 1683–1690, Aug. 2007.
14. Martin-Neira, M., D. M. LeVine, Y. Kerr, N. Skou, M. Peichl, A. Camps, et al., "Microwave interferometric radiometry in remote sensing: An invited historical review," *Radio Science*, Vol. 49, 415–449, Jun. 2014.
15. Torres, F., A. B. Tanner, S. T. Brown, and B. H. Lambrigsten, "Analysis of array distortion in a microwave interferometric radiometer: Application to the GeoSTAR project," *IEEE Transactions on Geoscience and Remote Sensing*, Vol. 45, 1958–1966, Jul. 2007.
16. Rautiainen, K., J. Kainulainen, T. Auer, J. Pihlflyckt, J. Kettunen, and M. T. Hallikainen, "Helsinki university of technology L-band airborne synthetic aperture radiometer," *IEEE Transactions on Geoscience and Remote Sensing*, Vol. 46, 717–726, Mar. 2008.

17. Wu, J., C. Zhang, H. Liu, and J. Y. Yan, "Performance analysis of circular antenna array for microwave interferometric radiometers," *IEEE Transactions on Geoscience and Remote Sensing*, Vol. 55, 3261–3271, Jun. 2017.
18. Lucotte, B. M., B. Grafulla-González, and A. R. Harvey, "Array rotation aperture synthesis for short-range imaging at millimeter wavelengths," *Radio Science*, Vol. 44, n/a-n/a, 2009.
19. Tanner, A., T. Gaier, W. Imbriale, P. Kangaslahti, B. Lambrigtsen, and B. Lim, "A dual-gain design for the geostationary synthetic thinned array radiometer," *IEEE Geoscience and Remote Sensing Letters*, Vol. 11, 1340–1344, Aug. 2014.
20. Zhou, X., H. J. Sun, J. W. He, and X. Lu, "NUFFT-based iterative reconstruction algorithm for synthetic aperture imaging radiometers," *IEEE Geoscience and Remote Sensing Letters*, Vol. 6, 273–276, Apr. 2009.
21. Fessler, J. A. and B. P. Sutton, "Nonuniform fast Fourier transforms using min-max interpolation," *IEEE Transactions on Signal Processing*, Vol. 51, 560–574, Feb. 2003.
22. Camps, A., M. Vall-Ilossera, I. Corbella, F. Torres, and N. Duffo, "Angular and radiometric resolution of Y-shaped nonuniform synthetic aperture radiometers for earth observation," *IEEE Geoscience and Remote Sensing Letters*, Vol. 5, 793–795, Oct. 2008.
23. Feng, L., Q. X. Li, K. Chen, Y. F. Li, X. L. Tong, X. Q. Wang, et al., "The gridding method for image reconstruction of nonuniform aperture synthesis radiometers," *IEEE Geoscience and Remote Sensing Letters*, Vol. 12, 274–278, Feb. 2015.
24. Li, S., X. Zhou, B. Ren, H.-J. Sun, and X. Lv, "A compressive sensing approach for synthetic aperture imaging radiometers," *Progress In Electromagnetics Research*, Vol. 135, 583–599, 2013.
25. Zhang, C., J. Wu, H. Liu, and J. Yan, "Imaging algorithm for synthetic aperture interferometric radiometer in near field," *Science China Technological Sciences*, Vol. 54, 2224–2231, 2011.
26. Chen, J., Y. Li, J. Wang, Y. Li, and Y. Zhang, "An accurate imaging algorithm for millimeter wave synthetic aperture imaging radiometer in near-field," *Progress In Electromagnetics Research*, Vol. 141, 517–535, 2013.
27. Butora, R., M. Martin-Neira, and A.-L. Rivada-Antich, "Fringe-washing function calibration in aperture synthesis microwave radiometry," *Radio Science*, Vol. 38, 15/1–15/15, 2003.
28. Tanner, A. B., B. Lambrigsten, T. Gaier, and F. Torres, *Near Field Characterization of the GeoSTAR Demonstrator*, Jet Propulsion Laboratory, National Aeronautics and Space Administration, Pasadena, CA, 2006.
29. Camps, A., A. Cardama, and D. Infantes, "Synthesis of large low-redundancy linear arrays," *IEEE Transactions on Antennas and Propagation*, Vol. 49, 1881–1883, Dec. 2001.